

Equilibrium faceting shapes for quasicrystals

Kevin Ingersent and Paul J. Steinhardt

Department of Physics, University of Pennsylvania, Philadelphia, Pennsylvania 19104

(Received 15 August 1988)

The equilibrium shapes (ES's) of icosahedral quasicrystals are analyzed for a wide class of lattice models which incorporate finite-range two-body interactions. Completely faceted shapes have been predicted for such models at temperature $T=0$. We prove that a number of simple shapes cannot be ES's for any model in this class for which the atomic interactions are constrained to be pure-attractive. This extends the result of Ho *et al.* [Phys. Rev. Lett. **59**, 1116 (1987)], who showed that the pentagonal dodecahedron, a shape observed in grains of icosahedral Al-Cu-Fe and Ga-Mg-Zn, is a forbidden shape for pure-attractive models. We then introduce a lattice model for quasicrystals which incorporates mixed attractive and repulsive interactions and show that the possible ES's include the dodecahedron and other previously forbidden shapes.

I. INTRODUCTION

Recently, several groups¹⁻⁵ have reported the discovery of icosahedral phases which have been observed to form large, single grains with smooth, flat facets. To date, two different faceting shapes have been observed: a rhombic triacontahedron, found¹⁻³ in Al₆Li₃Cu, and a pentagonal dodecahedron, exhibited by the Al-Cu-Fe system⁴ and the Ga-Mg-Zn system.⁵ In each case, calorimetric measurements indicate that the icosahedral phase is thermodynamically stable. The results strongly suggest that if the grains were grown in true equilibrium with the liquid phase, flat facets would remain, although the grain shape might be different.

The theory of equilibrium faceting has been extensively studied for crystals (see Ref. 6 and the references therein). The equilibrium shape (ES) is determined by minimizing the interfacial free energy as a function of orientation. This minimization procedure can be accomplished using the well-known Wulff construction.⁷ Herring^{8,9} and others^{10,11} have analyzed the possible ES's for crystal lattice models with short-range atomic interactions.

A number of different theoretical models of the icosahedral phase have been employed in attempts to explain the observed faceting. First, the Wulff construction has been applied to the quasicrystal model,^{12,13} which exhibits long-range quasiperiodic translational order. Flat faceting is predicted at temperature $T=0$ for two different lattice models of perfect quasicrystals with short-range interactions.^{14,15} It has been argued¹⁶ that any facet with a fivefold-symmetry axis is likely to remain smooth at all temperatures. Second, faceting has been analyzed for quasicrystals with a finite density of dislocation defects.¹⁷ It has been suggested that "rounded" facets occur, where the radius of curvature of the facets decreases with increasing defect density. A mean dislocation separation of 2000 Å, which is consistent with the observed translational correlation length in the icosahedral alloy grains, yields facets whose curvature would be undetectable experimentally. Finally, the Wulff construction has been extended to a "quasiglass" mod-

el,¹⁴ a structure with finite-range translational correlations, and once again, faceted shapes are predicted at $T=0$. This model, which is probably too artificial to be a realistic model of the icosahedral phase, has been created as a theoretical counterexample to the notion that long-range translational order is required to obtain flat facets. It is unclear whether the result is relevant to the icosahedral glass model^{18,19} that has been proposed as an explanation of the icosahedral phase.

Numerous equilibrium faceting shapes have been derived in these studies. However, the primary emphasis has been on determining whether faceting occurs at all, rather than any systematic investigation of the possible ES's. Each of the studies has employed a lattice model with short-range *attractive* interactions of a type which leads to a particularly simple form for the interfacial free-energy density. In their Wulff-construction analysis of this form of free energy, Ho *et al.*¹⁴ showed that the ES of icosahedral quasicrystals and quasiglasses could not be a pentagonal dodecahedron, although the shape might arise in nonequilibrium growth processes.

The purpose of this paper is to extend the $T=0$ Wulff-construction faceting analysis to a wider class of quasicrystal lattice models, which incorporate both attractive and repulsive atomic interactions. Repulsion can arise within a material because of intrinsic two-body repulsive forces (e.g., ionic interactions) or steric crowding of atoms in their local environments. Our original motivation was to consider whether the selection rule against the pentagonal dodecahedral ES extends to the wider class of models. The issue has immediate experimental relevance because, as mentioned above, pentagonal dodecahedral faceting is observed in icosahedral alloys. Our conclusion, briefly reported elsewhere,²⁰ is that there is no such selection rule: The pentagonal dodecahedron is a permissible ES over a wide range of parameters, once repulsive interactions are introduced.

In this paper we present a more general analysis of the role of repulsive interactions in determining faceting shapes. We show that repulsive interactions have somewhat different consequences for quasicrystals than for

periodic crystals. We illustrate several faceting shapes, in addition to the pentagonal dodecahedron, which cannot occur in models with pure-attractive interactions, but which *are* attainable in systems with both attraction and repulsion between atoms.

In Sec. II we present a review of theory necessary for our subsequent argument. Then, in Sec. III we make some general observations about the Wulff shapes which may be obtained from models which incorporate only short-ranged attractive two-body forces. In Sec. IV we describe our model for the surface energetics of quasicrystals. Possible ES's for icosahedral systems are presented in Sec. V, and their relevance to experiment is discussed in Sec. VI.

II. THE STANDARD METHOD OF COMPUTING EQUILIBRIUM SHAPES

A. Wulff construction

For a general survey of the thermodynamic formulation of the ES problem, the reader is referred to the review by Rottman and Wortis.⁶ In this section we remind the reader of those technical details of the theory that are crucial to our results. Much of the work presented here is due to Herring.^{8,9}

Our starting point is the free-energy density for formation of an infinite plane interface between coexisting solid and fluid phases. This depends on the temperature, T , and the orientation of the interface with respect to the crystal axes. Given the value of the surface free-energy density $\gamma(\hat{n}, T)$ as a function of the direction of the outward unit normal, \hat{n} , the shape of a macroscopic sample of the solid at fixed T can be found graphically by the Wulff construction.⁷ In three dimensions (3D), the ES is found by the following steps: (1) Make a polar plot of $\gamma(\hat{n}, T)$ as a function of the direction of \hat{n} . (2) For each point of this γ plot, construct an infinite plane perpendicular to the radius vector at that point. (3) The inner envelope of all such planes has the same shape as the ES at temperature T .

For illustrative purposes, it is convenient to consider the ES problem in two dimensions (2D). The Wulff construction in 2D involves the same steps as in 3D, with the obvious difference that a *line*, rather than a *plane*, is drawn perpendicular to the radius at every point of the γ plot. An example of this construction is shown in Ref. 8, Fig. 1. Quite generally, in 2D or 3D, the γ plot consists of smooth regions meeting at cusps, where the derivatives of the plot vary discontinuously. Each cusp can result in an extended flat surface, or facet, normal to the cusp direction. Smoothly varying portions of the γ plot can contribute regions of the ES where the normal to the surface varies continuously. Parts of the γ plot which do not contribute to the ES (that is, the normals to the radius vector do not lie on the inner envelope) are said to be *passive*. A plane surface normal to any passive direction is unstable with respect to local rearrangement into a "hill-and-valley" formation made up only of surfaces with normal orientations found in the ES.

Herring⁸ has formalized these and other observations concerning the relationship between the γ plot and the

ES. We quote here a theorem which determines whether or not there exists in the three-dimensional ES a facet normal to a particular direction. (For 2D, replace the word "sphere" with "circle".)

Theorem 1 (Herring). To ensure that the surface of the equilibrium shape has a flat portion of finite extent and with an orientation normal to a given vector OA of the γ plot, it is necessary and sufficient that the γ plot have a pointed cusp at A and simultaneously that there be some sphere through A and the origin which lies entirely inside the γ plot.

For most lattice models of perfect crystals in 3D, it is found that along the symmetry directions the γ plot at low T has cusps so pronounced that every point on the smoothly varying regions of the γ plot is rendered passive. Thus the ES is polyhedral, with sharp corners and edges. As the temperature is raised, the cusps are weakened by the effects of thermal fluctuations, allowing the formation of rounded surfaces between the facets. Each facet has a roughening temperature, above which its cusp becomes smoothed out, and the facet itself vanishes. Beyond the highest roughening temperature (assuming that this temperature is below the melting temperature of the solid), the ES is everywhere completely smooth.

B. γ plot constructed from sections of spheres

For the remainder of this paper we shall consider only atomic structures in which the effective interactions are finite-range two-body forces, so that the bulk cohesive energy of the solid can be written as a sum over pairwise bonds. We assume that the bonds can be divided into a finite number of sets, labeled by i , whose members have identical lengths l_i and directions \hat{A}_i , each bond requiring energy ϵ_i to be broken. The number of bonds of type i cut by a flat surface of area S , with unit outward normal \hat{n} , is $S l_i \rho_i |\hat{n} \cdot \hat{A}_i| + \text{corrections}$, where ρ_i is the average volume density of bonds of type i . Provided that the local density of bonds of each type is sufficiently uniform throughout the material, the corrections may be neglected in the limit of macroscopic S , and the number of bonds cut will be invariant under translations of the surface parallel to \hat{n} . Then the surface energy per unit area is

$$\epsilon(\hat{n}) = \sum_i (\epsilon_i l_i \rho_i) |\hat{n} \cdot \hat{A}_i| .$$

Expressions of this form arise in a wide class of lattice models.⁸ Thus, in addressing the $T=0$ faceting problem, it is natural to concentrate on surface free energies of the form

$$\gamma(\hat{n}) = \sum_{i=1}^N g_i |\hat{n} \cdot \hat{A}_i| , \quad (1)$$

where the unit vectors \hat{A}_i depend on the bond directions and the details of the model, and the coefficients g_i are functions of the strength and sign of the interactions. (We have dropped the explicit temperature dependence of the surface free energy. Henceforth, it will be assumed that $T=0$.)

If all possible normal vectors \hat{n} are placed tail to tail at

some point in space, their heads describe a sphere of unit radius. The surface of this sphere may be partitioned by the construction of a set of great circles, one perpendicular to each vector \hat{A}_i entering Eq. (1). This construction, illustrated in Fig. 1(a), divides the surface into spherical polygons. Herring used the term *pyramid* to describe the region of solid angle subtended at the origin of the sphere by such a polygon. Within any pyramid p , none of the terms $\hat{n} \cdot \hat{A}_i$ changes sign, so there exists a vector s_p such that

$$\gamma(\hat{n}) = \hat{n} \cdot s_p. \quad (2)$$

The point s_p will be called the *pole* of pyramid p . The

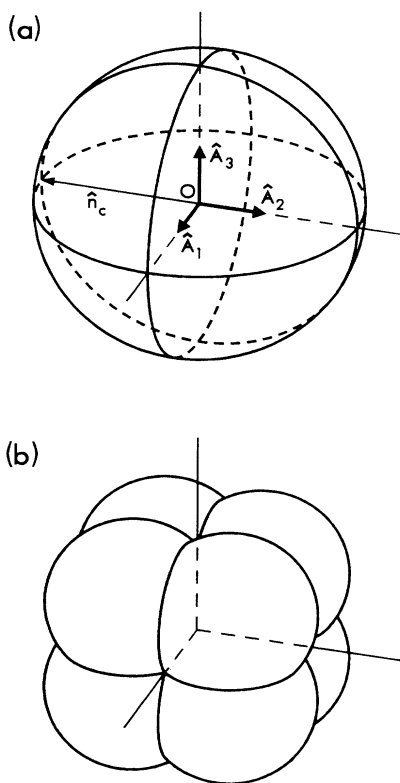


FIG. 1. Illustration of the Wulff construction described in Sec. II B for a simple lattice model with cubic symmetry. (a) The unit sphere of normal orientations, \hat{n} , to the surface of the equilibrium shape. A great circle is constructed perpendicular to each of the three bond directions \hat{A}_i (which lie along three mutually perpendicular crystal axes). This construction divides the surface of the sphere into eight spherical triangles, and divides the solid angle about the origin, O , into eight "pyramids." The intersection of any two great circles, such as at \hat{n}_c , gives rise to a point cusp in the γ plot along direction \hat{n}_c from the origin. (b) The Wulff plot corresponding to (a). Within each of the eight pyramids, the surface of the γ plot coincides with the surface of the sphere on which the origin and the pole of the pyramid are to be found at diametrically opposite points. (The poles lie along the $\langle 111 \rangle$ directions.) The cusps in the surface produced by the intersection of the spheres lie along the three axes.

origin O and the pole s_p lie at diametrically opposite positions on the sphere of radius $\frac{1}{2}|s_p|$, centered at $\frac{1}{2}s_p$. Within pyramid p , the γ plot coincides with the surface of this sphere. The boundary between adjacent pyramids p and p' is marked by a knife-edge cusp of the γ plot, along which

$$\hat{n} \cdot s_p = \hat{n} \cdot s_{p'}.$$

Therefore, the γ plot is made up of sections of spheres which join continuously, but not smoothly [see Fig. 1(b)].

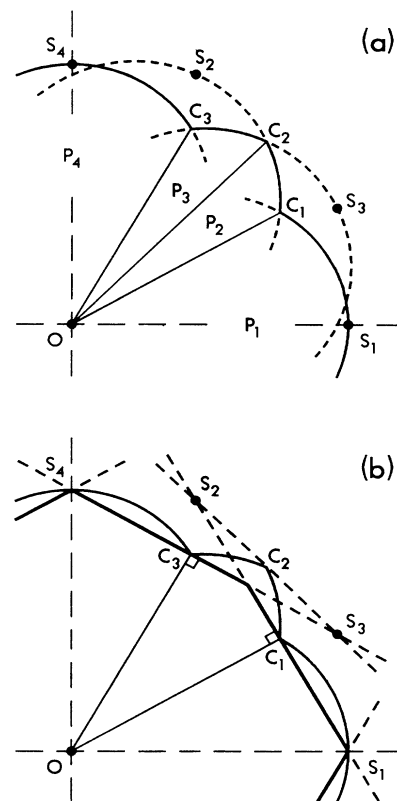


FIG. 2. One quadrant of the γ plot for a two-dimensional system having fourfold rotational symmetry. In both (a) and (b) the lines OS_1 and OS_4 are mirror planes. (a) Within each of the pyramids P_i , the surface of the γ plot (solid curve) coincides with the circle (dashed curve) which has the origin, O , and the pole, S_i , at diametrically opposite positions. At the boundaries between pyramids there exist cusps, labeled C_i , which may point inward or outward. An outward-pointing cusp (in this example, C_2) is always formed when the poles (S_2 and S_3) of two adjacent pyramids (P_2 and P_3) each lie on the side of the pyramid interface opposite the respective pyramid. (b) Construction of the equilibrium shape. A line is drawn through each cusp C_i , oriented perpendicular to OC_i . Irrespective of whether the cusp points inward or outward, the line passes through the poles of the pyramids which meet at the cusp. The equilibrium shape (drawn with a heavy solid line) is the envelope of these lines. Where the lines extend beyond the inner envelope, they have been drawn as dashed lines. Notice that the outward-pointing cusp, C_2 , does not contribute an edge to the equilibrium surface.

The corners of pyramids lie along directions in which there is an intersection between two or more great circles, i.e., along directions given by

$$\hat{\mathbf{n}}_c = \pm \hat{\mathbf{A}}_i \times \hat{\mathbf{A}}_j / |\hat{\mathbf{A}}_i \times \hat{\mathbf{A}}_j| ,$$

for any $i \neq j$. Associated with each such intersection there is a point cusp in the γ plot, at position $\mathbf{c} = \hat{\mathbf{n}}_c \gamma(\hat{\mathbf{n}}_c)$. The pole $\mathbf{s}_{p'}$ of every pole p' having a corner at $\hat{\mathbf{n}}_c$ satisfies

$$\hat{\mathbf{n}}_c \cdot \mathbf{s}_{p'} = \hat{\mathbf{n}}_c \cdot \mathbf{c} = \gamma(\hat{\mathbf{n}}_c) . \quad (3)$$

Equation (3) implies that the poles $\mathbf{s}_{p'}$ are coplanar with the cusp \mathbf{c} , which lies along the direction of $\hat{\mathbf{n}}_c$.

When the Wulff construction is carried out for a γ plot made up of sections of spheres, the plane drawn perpendicular to the radius at any point within any pyramid p passes through the corresponding pole \mathbf{s}_p . It can then be shown that the inner envelope of the construction is completely determined by the point cusps, resulting in a polyhedral ES. All smoothly curved regions of the γ plot are passive.

In 2D, Eq. (2) still holds, but the "two-dimensional pyramid" is a range of polar angles, and the corresponding region of the γ plot is a sector of the circle on which the origin O and the pole \mathbf{s}_p lie at diametrically opposite positions. Each two-dimensional pyramid lies between two neighboring pyramids, the intersections with which give rise to two cusps of the γ plot; each cusp \mathbf{c} is collinear with the poles of the two pyramids which intersect to form it. These features are illustrated in Fig. 2, which shows part of a γ plot. This sector of the plot is made up of four circular portions with poles at the points labeled S_i . The cusps formed by the meeting of the circular arcs fall into two categories: those like C_1 and C_3 , which are pointed towards the origin of the polar plot, and cusps such as C_2 , which point outward. No circle drawn through the origin and an outward-pointing cusp can lie entirely within the γ plot; therefore, by theorem 1, there cannot be an equilibrium facet normal to the direction of such a cusp. In other words, the ES for a system with a γ plot made up of portions of circles (spheres in 3D) is completely determined by the positions of the inward-pointing cusps.

III. FACETING WITH PURE-ATTRACTIVE BOND INTERACTIONS

Let us restrict $\gamma(\hat{\mathbf{n}})$ to be of the form of Eq. (1), with the further condition that all the coefficients g_i be positive. This situation arises at $T=0$ for a broad class of microscopic models which incorporate pure-attractive two-body forces.

Two recently published^{14,15} models for icosahedral quasicrystals with nearest-neighbor interactions were shown to result in $\gamma(\hat{\mathbf{n}})$ of the form

$$\gamma(\hat{\mathbf{n}}) = g \sum_{i=1}^N |\hat{\mathbf{n}} \cdot \hat{\mathbf{A}}_i| , \quad (4)$$

where the unit vectors $\hat{\mathbf{A}}_i$ have icosahedral point-group symmetry. In this special case, Ho *et al.*¹⁴ concluded

that the ES could never be the icosahedron or the pentagonal dodecahedron. Their argument was based on the observation that the Wulff construction for Eq. (4) results in an ES with a vertex at every pole position \mathbf{s}_p . Ho *et al.* then showed that a necessary condition for a convex polyhedron to be the ES for some set of $\hat{\mathbf{A}}_i$'s is that there exists a set of great circles, such that every intersection between the circles coincides with a vertex direction of the polyhedron. This condition cannot be fulfilled for an icosahedron or a dodecahedron.

We shall address the more general question of whether a given shape can be the ES of any model having $\gamma(\hat{\mathbf{n}})$ of the form of Eq. (1) with more than one coefficient g_i , each of which is constrained to be positive (i.e., pure-attractive interactions). Our Wulff-construction analysis will be valid for materials having crystalline or quasicrystalline translational order, and bond-orientational order of arbitrary symmetry. The results we obtain will then be applied to the case of icosahedral symmetry.

A. Wulff analysis for arbitrary symmetries

Herring has pointed out⁸ that if $\gamma(\hat{\mathbf{n}})$ is given by Eq. (1) with all coefficients positive, then for any direction of $\hat{\mathbf{n}}$ the pyramid $p(\hat{\mathbf{n}})$ within which $\hat{\mathbf{n}}$ lies gives a larger value of $\hat{\mathbf{n}} \cdot \mathbf{s}_p$ than any other pyramid, p' :

$$\hat{\mathbf{n}} \cdot \mathbf{s}_{p(\hat{\mathbf{n}})} > \hat{\mathbf{n}} \cdot \mathbf{s}_{p' \neq p(\hat{\mathbf{n}})} . \quad (5)$$

Equation (5) implies that for any $\hat{\mathbf{n}}$ the γ plot is the outermost surface which can be chosen from among the spheres defined by Eq. (2):

$$\gamma(\hat{\mathbf{n}}) = \sup_p \hat{\mathbf{n}} \cdot \mathbf{s}_p . \quad (6)$$

This excludes the possibility of an outward-pointing cusp of the type discussed in Sec. II, since in the vicinity of such a cusp there must be sections of the spheres forming the cusp which lie farther from the origin than the surface of the γ plot [see Fig. 2(a)]. With this observation, we are able to prove the following theorem.

Theorem 2. When $\gamma(\hat{\mathbf{n}})$ is of the form of Eq. (1) with all the coefficients $g_i > 0$, there is a one-to-one correspondence between the point cusps of the γ plot and the facets of the Wulff shape. The direction of each cusp, $\hat{\mathbf{n}}$, is identical to the outward normal direction to the corresponding facet.

Proof. Theorem 1 states that each facet is normal to the direction of some point cusp of the γ plot. We now have to show that the relationship is one to one, i.e., that there is a facet normal to every cusp direction. Consider a point cusp \mathbf{c} of the γ plot lying along direction $\hat{\mathbf{n}}_c$ from the origin. Let there be m pyramids p' having a corner at $\hat{\mathbf{n}}_c$, and pole $\mathbf{s}_{p'}$ satisfying Eq. (3). We calculate the center-of-mass position of these poles, which is

$$\mathbf{s}_c = \frac{1}{m} \sum_{p'} \mathbf{s}_{p'} ,$$

and construct the sphere defined in polar coordinates by

$$r_c(\hat{\mathbf{n}}) = \begin{cases} \hat{\mathbf{n}} \cdot \mathbf{s}_c = (1/m) \sum_{p'} \hat{\mathbf{n}} \cdot \mathbf{s}_{p'} & \text{for } \hat{\mathbf{n}} \cdot \mathbf{s}_c \geq 0, \\ 0 & \text{otherwise.} \end{cases} \quad (7)$$

This sphere passes through the origin and the cusp \mathbf{c} . Using Eqs. (5)–(7), it can be shown that the sphere lies entirely within the γ plot, except at \mathbf{c} itself. According to theorem 1, the existence of such a sphere is a sufficient condition for the ES to exhibit a finite facet normal to $\hat{\mathbf{n}}_c$. This argument was developed quite generally for any cusp, so we have proved the one-to-one relationship between cusps and facets. Q.E.D.

The directions of the cusps in $\gamma(\hat{\mathbf{n}})$ are completely determined, through the great-circle construction, by the choice of vectors $\hat{\mathbf{A}}_i$ entering Eq. (1). Therefore, we can state a

Corollary to theorem 2. Suppose that $\gamma(\hat{\mathbf{n}})$ is of the form of Eq. (1) with all $g_i > 0$. A necessary, but not sufficient, condition for a given faceted shape to be a possible equilibrium shape is that there exists a set of great circles whose intersections are in one-to-one correspondence with the facets, and such that each intersection lies along the outward normal direction to a facet.

The condition is not *sufficient* for the following reason. Complete description of a polyhedral shape requires that one specify (in addition to the outward normal direction to each facet) the relative sizes of the facets which depend on the radius from the origin of each cusp. Even though a polyhedron may satisfy the condition on the normal directions of its facets, we have not proved that there exists a choice of positive g_i 's which correctly reproduces the relative sizes of its facets.

A more concise statement of the restriction on possible ES's may readily be proved from the corollary to theorem 2: For the class of pure-attractive lattice models we have considered, any ES has to be a zonohedron—a convex polyhedron in which each face has a center of inversion symmetry.²¹ This result enables many potential ES's to be eliminated, simply because they exhibit facets with an odd number of edges.

B. ES's of icosahedral systems

We now specialize to the case of systems with icosahedral orientational symmetry. A generalization of Eq. (4) which may include the effects of next-nearest-neighbor, or indeed any finite-range, two-body attractive forces is

$$\gamma(\hat{\mathbf{n}}) = \sum_{\mu=1}^M g^{(\mu)} \sum_{\alpha=1}^{N_{\mu}} |\hat{\mathbf{n}} \cdot \hat{\mathbf{A}}_{\alpha}^{(\mu)}|, \quad (8)$$

where the unit vectors $\hat{\mathbf{A}}_{\alpha}^{(\mu)}$ can be arranged in finite sets, $\mathcal{A}^{(\mu)} = \{\hat{\mathbf{A}}_{\alpha}^{(\mu)}, \alpha = 1, \dots, N_{\mu}\}$, each exhibiting icosahedral symmetry. Once again, the coefficients $g^{(\mu)}$ are restricted to be positive.

At this point we provide a more precise definition of what is meant by an “icosahedrally symmetric” set of vectors. A set of vectors which is said to have full icosahedral point-group symmetry is the union of *icosahedral orbits*. The orbit $\mathcal{O}(P)$ of a point P lying on

the surface of an icosahedron is defined as the set of images of P under the action of the full 120-element icosahedral group (Y_h or $m\bar{5}\bar{3}$). The same set of points may be generated starting from any member of the orbit. An orbit induces a representation of Y_h , in which each element of the group corresponds to a permutation of the orbit. The vectors in any icosahedral orbit lie in pairs on axes through the center of the icosahedron. Each axis will be taken to be a unit vector, its sense (parallel or antiparallel to either one of the pair of orbit vectors) being determined by arbitrary convention. Taken together, these axes comprise the *icosahedral axis set* $\mathcal{A}(P)$ generated by P .

The number of elements in $\mathcal{O}(P)$, and consequently the number of axes in $\mathcal{A}(P)$, depends on the precise position of P on the icosahedron. We list below the five categories of icosahedral axis sets and the symbol used to denote each. The positions of the generators for cases (1)–(4) are illustrated in Fig. 3.

- (1) The set of six fivefold axes, V_6 , generated by P lying at a vertex of the icosahedron.
- (2) The set of ten threefold axes, F_{10} , generated by P lying at a face center.
- (3) The set of 15 twofold axes, E_{15} , generated by P lying at an edge center.
- (4) The set of 30 axes, M_{30} , generated by P lying on a mirror plane of the icosahedron, where P is not also one of the points of rotational symmetry. There is a continuum of such points, so a particular set is specified by the location of a generating point. We shall refer to the following sets: (a) $M_{30}^{(1)}$, generated by a point lying a fraction $3(3-\tau)/10$ of the way along the line from a vertex of the icosahedron to the center of any face adjacent to that vertex; (b) $M_{30}^{(2)}$, generated by a point lying at the

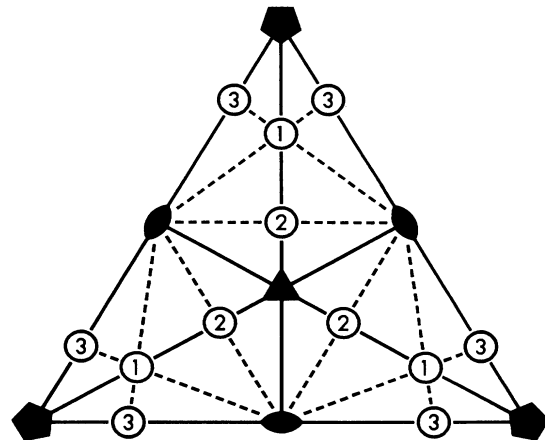


FIG. 3. One face of an icosahedron, showing generators of the six icosahedral axis sets referred to in the text. The standard stereographic symbols indicate the fivefold, threefold, and twofold rotation axes, which generate the axis sets V_6 , F_{10} , and E_{15} , respectively. The solid lines connecting these axes represent mirror planes of the icosahedron. The circled digits indicate points which generate the axis sets $M_{30}^{(1)}$, $M_{30}^{(2)}$, and $M_{30}^{(3)}$.

midpoint of the line connecting the centers of any two edges which bound the same face of the icosahedron; (c) $M_{30}^{(3)}$, generated by a point lying on an edge of the icosahedron, a fraction $(2\tau^2)^{-1}$ of the way along the edge from either end. [The symbol τ represents the golden mean, $\frac{1}{2}(\sqrt{5}+1)$.]

(5) The set of 60 axes generated by any point P on the icosahedron which does not give rise to one of the sets in (1)–(4). Once again, there is a continuum of such points. We shall not need to refer to this case again.

Icosahedral orbits and axis sets will appear throughout our discussion in classifying different features of the icosahedral faceting problem. For instance, the vectors $\hat{\mathbf{A}}_\alpha^{(\mu)}$ in Eq. (8), which appear only in the form $|\hat{\mathbf{n}} \cdot \hat{\mathbf{A}}_\alpha^{(\mu)}|$, can be expressed as the union of icosahedral axis sets. The cusps of the γ plot lie along directions

$$\pm \hat{\mathbf{A}}_\alpha^{(\mu)} \times \hat{\mathbf{A}}_\beta^{(\nu)} / |\hat{\mathbf{A}}_\alpha^{(\mu)} \times \hat{\mathbf{A}}_\beta^{(\nu)}|. \quad (9)$$

Since point-group operations preserve the lengths of, and angles between, the axis vectors, the set of all cusp directions must be decomposable into one or more icosahedral orbits.

In addition, the set of outward normal directions to the faces of any icosahedrally symmetric polyhedron must be decomposable into icosahedral orbits. Therefore, the number of facets exhibited by the ES, N_f , can take only certain values, which may be derived from the above list of icosahedral axis sets. The eight lowest permitted values of N_f are

$$N_f = 12, 20, 30, 32, 42, 50, 60, 62. \quad (10)$$

(All other values may be obtained from these eight by adding integral multiples of 60.)

Returning to the Wulff analysis, one concludes from the corollary to theorem 2 that the ES of the model under consideration can never be an icosahedron ($N_f = 12$) or a pentagonal dodecahedron ($N_f = 20$), because these shapes are not zonohedra. Any set of great circles whose intersections include outward normal directions corresponding to each face of an icosahedron or a dodecahedron necessarily has many additional intersections. These additional intersections lead to additional facets (beyond those for the icosahedron or dodecahedron). In other words, there exists no union of sets $A^{(\mu)}$ of icosahedral axis vectors such that the cusp directions in Eq. (9) may be completely organized into pairs, one along each axis in V_6 or F_{10} . This extends the validity of the result of Ho *et al.* for a single coupling to the case of arbitrarily many $g^{(\mu)}$'s.

The Wulff shape produced by the icosahedral set with fewest vectors, $A^{(1)} = V_6$, is the 30-faceted rhombic triacontahedron.¹⁴ Increasing the number of vectors in Eq. (8) always results in a γ plot with a greater number of cusps and hence, by theorem 2, an ES with more than 30 facets. Indeed, the next lowest number of facets which can be obtained is $N_f = 62$: the great rhombicosidodecahedron [see Fig. 4(c)], produced by the choice $A^{(1)} = E_{15}$. Thus, the first two, and six of the first eight, members of the sequence in Eq. (10) are not attainable with pure-attractive interactions. This contrasts with the

crystallographic symmetries, for which the fewest-faceted shape is a zonohedron. For instance, in the cubic system, the cube is a possible ES. Note, however, that the octahedron may not be obtained as the ES of a pure-attractive cubic lattice model.

IV. LATTICE MODELS WITH MIXED ATTRACTIVE AND REPULSIVE INTERACTIONS

One is prompted by the results of the preceding section to consider whether or not the range of possible equilibrium shapes might be extended by permitting negative coefficients in the expression for the macroscopic interfacial free-energy density [Eqs. (1) and (8)]. On the microscopic level, this corresponds to incorporating into our model repulsive, as well as attractive, interactions. Physically, repulsion may arise because of inherently repulsive finite-range two-body forces, such as screened electrostatic repulsion between cations. In addition, steric crowding of individual atoms, or clusters of atoms, may result in effective two-body repulsion.

We defer further discussion of possible ES's until the next section. At this point we describe a microscopic toy model for three-dimensional quasicrystals which includes repulsive effects, and demonstrate that it yields an expression for the interfacial free-energy density which is of the form of Eq. (8) with coefficients of mixed sign. Our model is a generalization of the lattice-gas model for quasicrystal faceting introduced by Garg and Levine.¹⁵ The model can be defined in two stages, which will be described, in turn, in the following subsections. Briefly, the generalized dual method²² (GDM) is employed to create a packing of unit cells. Then we specify an atomic decoration of the cells, and bond energies between the cells, so as to arrive at an expression for the energy density of a flat interface. (It is in this second respect that the theory of Garg and Levine differs from that of Ho *et al.*¹⁴)

The magnitude of the repulsive interactions which may be included in the model is limited by the requirement that the material be stable, in a limited sense which will be defined here. It is an assumption built into all such atomic lattice models, crystalline or quasicrystalline, that there exist interatomic forces such that each atom is stable with respect to local deviations from its lattice site. No further assumption is made about the form of these forces, other than the resulting bond energies, which describe the net energy required to move two atoms from their lattice positions to infinite separation. Therefore, we are unable to address the stability of the material with respect to arbitrary changes in the positions of the atoms. When repulsive bonds are included in the model, only two checks of bulk stability can be made: that both the free energy to completely dissociate all the bonds, and the net cost of creating a cleavage surface within the material, remain positive.

Ideally, one would proceed by analogy to the case of perfect crystals, for which it is possible to construct lattice models^{8–10} in which the next-nearest-neighbor bonds are repulsive, while bulk stability is maintained by the presence of attractive nearest-neighbor bonds. However, the vast number of different local configurations occurring within a quasicrystal greatly complicates any calcu-

lation involving effects beyond nearest-neighbor range. Therefore, we assume that only “contact” forces exist, and choose some of these to be repulsive. While this model may not be physically very realistic, it nonetheless reproduces many macroscopic features of next-nearest-neighbor models, and has the advantage of tractability.

A. Quasicrystal structure

In this subsection we review the use of the GDM to generate three-dimensional quasicrystals,²² and discuss certain important features of the structures so produced. The GDM begins with the construction of a *grid* of infinite planes perpendicular to each member of a *star* of unit vectors, $\mathcal{E} = \{\hat{\mathbf{e}}_i, i = 1, \dots, N\}$. The planes belonging to grid i may be labeled with an integer in sequence of their positions along the $\hat{\mathbf{e}}_i$ direction. These planes may be periodically or quasiperiodically spaced; in either case the unit of spacing is some length b_i . The grids divide grid space into open volumes, each of which may be uniquely labeled by a set of N integers k_i defined as follows: any point lying within the open volume in question falls between the planes from grid i having labels k_i and $k_i + 1$. Then the dual construction maps each volume in grid space onto a lattice point in real space at $\sum_{i=1}^N k_i a_i \hat{\mathbf{e}}_i$, where a_i is the length of all lattice edges parallel to $\hat{\mathbf{e}}_i$. The result is a space-filling arrangement of parallelepipeds, each of which is dual to an intersection between three grid planes.

The orientational symmetry of a quasicrystal produced using the GDM depends on the choice of star vectors $\hat{\mathbf{e}}_i$ and their associated real- and grid-space lengths, a_i and b_i . In order that the quasicrystal diffraction pattern be invariant under the symmetry operations of some point group G , the star \mathcal{E} should decompose into subsets, each of which is a G -symmetric axis set, and within which a_i and b_i are independent of i . The number of different unit-cell shapes is determined by the number of distinct triplets of edge vectors $a_i \hat{\mathbf{e}}_i$. For example, the star with fewest vectors which produces an icosahedral packing is the set $\mathcal{E} = V_6$, with $a_i = a$ and $b_i = b$ for all i . There result two different cell shapes, the minimum possible number for a quasicrystal. With this star, the value of a determines the overall scale of the quasicrystal, while the magnitude of b has no physical significance. Generally, if \mathcal{E} has M distinct symmetric subsets, with $M > 1$, one introduces $M - 1$ constants which fix the ratios of the a_i 's between subsets. Varying these constants affects the relative sizes and aspect ratios of the cells in the packing, and consequently changes the positions of peaks in the diffraction pattern. The ratios of the b_i 's provide a further $M - 1$ degrees of freedom which determine the relative number of occurrences of different cell shapes, and the relative intensities of various diffraction peaks. We remind the reader that quasicrystal lattices produced by periodic or quasiperiodic grid spacing have the same cell shapes, but may differ in the configuration of cells, and the relative numbers of the various shapes.

One feature of all three-dimensional quasicrystals constructed using the GDM is the existence of *rails*:²³ one-dimensional sequences of cells, connected by identically

shaped parallel faces. Each rail is dual to a line of intersection between two grid planes. In grid space, any two planes belonging to different grids, say j and k , intersect along a straight line L parallel to $\hat{\mathbf{e}}_j \times \hat{\mathbf{e}}_k$. The intersection between this line and any third grid plane, perpendicular to $\hat{\mathbf{e}}_l$ ($l \neq j, k$), say, is dual to a cell in which two opposite faces are oriented perpendicular to $\hat{\mathbf{e}}_j \times \hat{\mathbf{e}}_k$; these faces are related by a translation through $\pm a_l \hat{\mathbf{e}}_l$. Successive intersection points along L produce a rail. The average direction of translation, $\hat{\mathbf{q}}$, as one moves from the center of one shared face to the next along the rail depends on the orientation and relative separation of the grid planes which intersect L . In a system with a high degree of rotational symmetry, such as an icosahedral packing, the average rail direction is just the normal to the connecting faces, i.e.,

$$\hat{\mathbf{q}} \equiv \hat{\mathbf{q}}_{jk} = \hat{\mathbf{e}}_j \times \hat{\mathbf{e}}_k / |\hat{\mathbf{e}}_j \times \hat{\mathbf{e}}_k|. \quad (11)$$

L is one of an infinite set of parallel lines of intersection between elements from grids j and k . Hence, there exists a *family* of nonintersecting “parallel” rails, labeled $[j, k]$, with the same average direction in real space. We have already seen that if the point group of the system is G , the star must be the union of G -symmetric axis sets. Consider the set of all rail directions, $\{\hat{\mathbf{q}}_{jk}\}$, obtained from such a star by using Eq. (11). (We do not distinguish between $\hat{\mathbf{q}}_{jk}$ and $-\hat{\mathbf{q}}_{jk}$.) Since operations of the point group G preserve the lengths of, and angles between, the star vectors, the set $\{\hat{\mathbf{q}}_{jk}\}$ must also be decomposable into G -symmetric axis sets.

Each cell in the quasicrystal lies at the intersection of three nonparallel rails. Since a quasicrystal constructed from a star with N vectors has $\frac{1}{2}N(N-1)$ families of rails, any one family of rails can pass through only a fraction of the cells. Rather than directly computing this fraction, it is convenient to define the *rail density* σ_{jk} : the mean area density of rails in $[j, k]$, measured in a plane normal to $\hat{\mathbf{q}}_{jk}$. It can be shown that this density depends on the orientations of the star vectors, as well as the a_i 's and b_i 's, through the formula

$$\sigma_{jk} = |\mathbf{d}_{jk} \times \mathbf{d}_{kj}|^{-1}, \quad (12)$$

where

$$\mathbf{d}_{lm} = \eta_{lm}^{-1} \sum_{n=1}^N \eta_{ln} a_n \hat{\mathbf{e}}_n \quad (13)$$

with

$$\eta_{pq} = [\hat{\mathbf{e}}_p \times (\hat{\mathbf{e}}_j \times \hat{\mathbf{e}}_k)] \cdot \hat{\mathbf{e}}_q / b_q. \quad (14)$$

In order to check the bulk stability of the material, we shall also need an expression for the *face density* ρ_{jk} : the average volume density of faces which are shared between cells in $[j, k]$. This density is given by

$$\rho_{jk} = |\mathbf{d}_1 \cdot \mathbf{d}_{jk} \times \mathbf{d}_{kj}|^{-1}, \quad (15)$$

where \mathbf{d}_{jk} and \mathbf{d}_{kj} are given by Eq. (13), and

$$\mathbf{d}_1 = \sum_{n=1}^N \eta_{1n} a_n \hat{\mathbf{e}}_n / \sum_{n=1}^N \eta_{1n}, \quad (16)$$

with

$$\eta_{1n} = (\hat{e}_j \times \hat{e}_k) \cdot \hat{e}_n / b_n. \quad (17)$$

Note that ρ_{jk} is also equal to the average volume density of cells which lie on rails belonging to $[j, k]$.

Table I lists properties of the rails present in an icosahedral quasicrystal constructed from a set of star vectors, \mathcal{E} , which is composed of any combination of the sets V_6 , F_{10} , and E_{15} . The list is organized according to which sets of grid planes intersect to form the rails. If \mathcal{E} is composed of only one axis set, $\mathcal{E} = \mathcal{A}$, then all the rails are produced by the intersection of planes normal to vectors belonging to \mathcal{A} . The set of all such rails is denoted in the left-hand column of the table by $\mathcal{A} \times \mathcal{A}$. When \mathcal{E} is the union of icosahedral axis sets (e.g., $\mathcal{E} = \mathcal{A}^1 \oplus \mathcal{A}^2$), then the rails are produced not only by the intersection of planes belonging to grid in the same axis set (i.e., $\mathcal{A}^1 \times \mathcal{A}^1$ and $\mathcal{A}^2 \times \mathcal{A}^2$), but also by intersections between planes from different axis sets ($\mathcal{A}^1 \times \mathcal{A}^2$). For each pair of axis sets, the families of rails produced by the intersection of their grids may be grouped into sets having a common shared face shape and directions which form an icosahedral axis set. Each line of the table gives one of the shared face shapes, the number of families of rail which exhibit the shape, and the icosahedral axis set to which the rails are parallel.

For those families of rails which arise from a star com-

posed of only one of the axis sets, the Table gives two additional pieces of information: the rail density, σ , which is the sum of σ_{jk} [Eqs. (12)–(14)] over all families $[j, k]$ with the same shared face shape and rail direction, and the face density, ρ , which is the sum of ρ_{jk} [Eqs. (15)–(17)] over all families with the same shared face shape, *irrespective* of rail direction. Both quantities are calculated for cell edges of unit length. (When the star is made up of two or more axis sets, ρ and σ depend on the ratios of real- and dual-space lengths between the axis sets, and there exists no one representative value for either quantity.) For example, the fourth line in Table I indicates that the intersections between grids planes which are normal to the E_{15} directions produce (among others) rails in which the shared faces are parallelograms with edges meeting at an angle of 36° . These rails belong to 30 families, each of which is parallel to one of the V_6 directions, i.e., there are five families parallel to each fivefold axis. The combined rail density of the five families parallel to any one of the fivefold axes is $\sigma = 0.1176$; the combined face density for all 30 families is $\rho = 0.9708$.

B. Surface energetics

One simple decoration of the quasicrystal involves the placement of an atom at the center of each unit cell, and the association of a “bond” with every face between adja-

TABLE I. Properties of rails arising from intersections between different sets of grids employed in the generalized dual construction for icosahedral quasicrystals. The table groups together all rails produced by the intersection of two grid planes, one from each of the icosahedral sets listed in the left-hand column. (The nomenclature for icosahedral axis sets is defined in Sec. III.) Each line of the table represents a set of families of rails, within which the shape of the shared cells faces is identical and the rail directions belong to the same icosahedral axis set. The angle θ is the smaller internal angle subtended by the edges of each shared (rhombic) face. The number of families belonging to each set equals the number of different pairs of grids, j and k , which produce rails with the particular face shape, oriented along one of the directions in the specified axis set. See the end of Sec. IV A for further details, and definitions of the face and rail densities, ρ and σ , respectively. [The symbol τ represents the golden mean, $\frac{1}{2}(\sqrt{5}+1)$.]

Intersecting grids	Shared faces			Families of rails		
	$\tan\theta$	θ (deg)	ρ	Number	Direction	σ
$V_6 \times V_6$	2	63.435	4.6165	15	E_{15}	0.2236
$F_{10} \times F_{10}$	$2/\sqrt{5}$	41.810	1.3207	15	E_{15}	0.0600
	$\sqrt{8}$	70.529	3.6502	30	$M_{30}^{(1)}$	0.0848
$E_{15} \times E_{15}$		36	0.9708	30	V_6	0.1176
		60	1.5250	30	F_{10}	0.1039
		72	1.5708	30	V_6	0.1902
		90	0.8967	15	E_{15}	0.0400
$V_6 \times F_{10}$	$2/\tau^2$	37.377		30	E_{15}	
	$2\tau^2$	79.188		30	E_{15}	
$V_6 \times E_{15}$	$1/\tau$	31.717		30	E_{15}	
	τ	58.283		30	E_{15}	
		90		30	$M_{30}^{(2)}$	
$F_{10} \times E_{15}$	$1/\tau^2$	20.905		30	E_{15}	
	$\sqrt{2}$	54.736		60	$M_{30}^{(1)}$	
	τ^2	69.095		30	E_{15}	
		90		30	$M_{30}^{(3)}$	

cent cells.¹⁵ [This decoration is not meant to be realistic, but only to provide a simple model for which $\gamma(\hat{\mathbf{n}})$ is calculable.] In general, the energy of such a bond might depend on the configuration of cells out to quite some distance from the bond. We make the nearest-neighbor approximation that the energy of a bond between adjacent cells depends only on the shape and orientation in space of the face shared by the cells. This implies that all faces between cells in the family of rails $[j, k]$ have the same energy, ϵ_{jk} . Since the mean density of such bonds is ρ_{jk} , given by Eqs. (15)–(17), the average bond energy density within the bulk (i.e., the net dissociation energy per unit volume) can be written

$$u = \sum_{\substack{k,j \\ k > j}} \rho_{jk} \epsilon_{jk} . \quad (18)$$

Consider cleaving the quasicrystal between unit cells to create a surface which, although microscopically uneven, is macroscopically flat with normal orientation $\hat{\mathbf{n}}$. The energy required for this process is the sum of the bond energies for all faces between cells which have been separated. We first examine the case when all bond energies are positive. Since rails follow a macroscopically straight path through the material, the surface energy is minimized when any rail with direction $\hat{\mathbf{q}}_{jk}$ satisfying $\hat{\mathbf{n}} \cdot \hat{\mathbf{q}}_{jk} \neq 0$ is cut in exactly one place, and any other rail is not cut at all. The total energy cost may be calculated from the number of cut rails belonging to each family. For a macroscopic surface of area S , oriented normal to $\hat{\mathbf{n}}$, the number of rails in $[j, k]$ which must be cut is $|\hat{\mathbf{n}} \cdot \hat{\mathbf{q}}_{jk}| S \sigma_{jk} [1 + O(S^{-1/2})]$, where σ_{jk} is the mean area density of rails, defined by Eqs. (12)–(14), and lengths are assumed measured in cell-edge units. Then the macroscopic interfacial energy density is

$$\epsilon(\hat{\mathbf{n}}) = \sum_{\substack{k,j \\ k > j}} (\epsilon_{jk} \sigma_{jk}) |\hat{\mathbf{n}} \cdot \hat{\mathbf{q}}_{jk}| .$$

At $T=0$ the energy and free energy are identical, so one can see that $\gamma(\hat{\mathbf{n}})$ is of the form of Eq. (1), with each bond direction $\hat{\mathbf{A}}_i$ in the equation corresponding to the direction of a family of rails in the lattice model.

As an example, we return to the quasicrystal constructed from the V_6 star of vectors, for which there are 15 possible rail directions, $\hat{\mathbf{q}}_{jk} \in E_{15}$. The shape and size of the connecting faces in the different families of rail are identical, and by symmetry, the face energies ϵ_{jk} and mean densities σ_{jk} must be independent of j and k . Thus,

$$\gamma(\hat{\mathbf{n}}) = (\epsilon\sigma) \sum_{\substack{k,j \\ k > j}} |\hat{\mathbf{n}} \cdot \hat{\mathbf{q}}_{jk}| ,$$

which fits the form of Eq. (4).

The principal aim of this section is the incorporation of repulsive interactions into the lattice model. One obvious approach is to assign a negative energy for cutting any rail belonging to a certain subset of all families of rails. However, the straightforward inclusion of “repulsive rails” leads to departures from Eq. (1) in the form of $\gamma(\hat{\mathbf{n}})$, arising from anomalous configurations adopted by

interfaces whose macroscopic tangent direction makes a small angle to a family of repulsive rails (i.e., $|\hat{\mathbf{n}} \cdot \hat{\mathbf{q}}_{jk}| \ll 1$). Rather than the surface following a path which cuts the fewest possible rails, as is the case for pure-attractive models, it may be energetically more favorable to zig-zag back and forth many times across each repulsive rail. The average distance along the surface between cuts across a repulsive rail may be as small as a few cell spacings, so the reduction in the interfacial energy density can be quite significant.

The zig-zag surfaces (at $T=0$) are clearly unphysical. They can be traced back to the fact that we have included only nearest-neighbor interactions in our model. In crystal lattice models, where each unit cell is identically coordinated, repulsion must be introduced through next-nearest-neighbor bonds, while the nearest-neighbor bonds are kept attractive. As it turns out, any choice for the relative strengths of the repulsive and attractive interactions which satisfies the stability criterion also ensures that zig-zag surfaces are suppressed. In quasicrystal models, which are constructed from two or more distinct unit cells, a stable lattice model which includes repulsive interactions may be constructed from nearest-neighbor bonds alone. We have intentionally excluded next-nearest-neighbor bonds to avoid calculational difficulties. This exclusion, though, permits zig-zag surfaces to become the surfaces with lowest energy. To eliminate this problem, we will impose the constraint that no surface can cut a rail more than once. We imagine that this constraint might be obtained dynamically, say, through step-step interactions that raise the energy of zig-zag surfaces, while leaving the energy of other surfaces unchanged. We will assume the existence of such interactions, and simply ignore the zig-zag surfaces in computing the minimal energy surface. The interactions have no other effect on the computation. With this understanding, the calculation of the minimum interfacial energy for a surface with a given macroscopic normal direction $\hat{\mathbf{n}}$ may be performed in exactly the same manner as when all rail energies are positive.

In order to incorporate repulsive interactions into an icosahedral model, while maintaining bulk stability, it is necessary that the possible rail directions decompose into *two or more* icosahedral axis sets, $A^{(\mu)}$, corresponding to two or more types of cell faces. At least one of the sets must be assigned a positive (attractive) bond energy. We have seen that, when the quasicrystal star \mathcal{C} is the set of fivefold axes, the rails belong to one icosahedral axis set, resulting in all cell faces having the same shape. Therefore, this star is unsuitable for a model with mixed interactions. If \mathcal{C} is instead chosen to be the set of twofold axes, it can be seen from Table I that there are four distinct face shapes and icosahedral subsets of rail directions: one subset with rail directions in E_{15} , two with directions in V_6 , and the last having directions in F_{10} . By symmetry, the bond energies ϵ_{jk} and rail densities σ_{jk} within each subset must take values $\epsilon^{(\mu)}$ and $\sigma^{(\mu)}$, respectively, independent of j and k . Therefore, $\gamma(\hat{\mathbf{n}})$ takes the form of Eq. (8) with the coefficients

$$g^{(\mu)} = \epsilon^{(\mu)} \sigma^{(\mu)} \quad (19)$$

unrestricted, apart from limits imposed by the requirement of stability. As discussed above, the stability conditions amount to demanding that the bulk dissociation energy u [given by Eq. (18)] be positive, and $\gamma(\hat{n})$ remains positive for all directions \hat{n} .

The set E_{15} is not the only icosahedral star which gives rise to more than one axis set of rail directions. For instance, consulting Table I once again, the set of threefold axes produces rails along the directions in E_{15} and $M_{30}^{(1)}$. Still greater variety can be obtained by employing a star which itself is composed of more than one icosahedral axis set. For example, combining the V_6 and E_{15} sets of star vectors, the rail directions include those which would arise from either subset alone, plus additional directions produced by intersections between two grid planes, one from each of the two subsets.

To summarize this section, we have shown that there exists a microscopic model for quasicrystals for which the macroscopic interfacial free-energy density is well defined and takes the form of Eq. (1). The coefficients g_i may be positive or negative and chosen independently of one another, subject to constraints imposed by the symmetry of the system [which force $\gamma(\hat{n})$ to take the more restricted form given in Eq. (8)], and the requirements for bulk stability.

V. FACETING WITH MIXED ATTRACTIVE AND REPULSIVE INTERACTIONS

We now provide a plausibility argument that the inclusion of repulsive interactions may provide a richer collection of possible ES's than in the pure-attractive case. Consider starting with $\gamma(\hat{n})$ given by Eq. (1), with all coefficients positive. From inspection of Eq. (1), it should be apparent that the addition of terms with negative coefficients g_i , representing repulsion, favors the formation of a plane surface normal to the corresponding directions \hat{A}_i . If the original γ plot has a cusp along a direction making a small angle to such an \hat{A}_i , then that cusp will be moved inwards by the additional term. On the other hand, any cusps of the original γ plot which are far from all the newly favored directions will be pushed outward relative to the average. As the magnitude of the negative coefficients is increased, cusps that originally pointed towards the center of the γ plot may be flattened, resulting in a reduction in the size of the corresponding Wulff facets. Eventually, cusps may be inverted so that they point outward, at which stage their facets vanish completely from the ES. Thus, the one-to-one correspondence between cusps and facets may be broken by the inclusion of repulsive interactions, and the corollary to theorem 2, which, applied to purely attractive interactions, may no longer hold true.

The remainder of this section will be devoted to examples of ES's calculated for icosahedral systems when mixed attractive and repulsive interactions are involved. We shall find that the ES need not be a zonohedron, so that shapes which were forbidden in the pure-attractive case are attainable in the mixed case. We shall concentrate on those shapes which have the fewest facets, because they are most likely to be observed experimentally.

In particular, we shall demonstrate how to obtain simple (in most cases equilateral) polyhedra for all but one of the N_f values listed in Eq. (10).

Once again, we emphasize that all the examples shown were constructed subject to the conditions that the bulk dissociation energy be positive and $\gamma(\hat{n})$ remain positive for all \hat{n} . The sets of directions $A^{(\mu)}$ and coefficients $g(A^{(\mu)}) \equiv g^{(\mu)}$ in Eq. (8) will be specified for each ES. Where appropriate, an interpretation will also be provided in terms of our microscopic model. For the most part, we shall work with a quasicrystal constructed with the E_{15} star (i.e., the 15 twofold axes of an icosahedron), which results in rails along the V_6 , F_{10} , and E_{15} directions (see Table I). It should be noted that a given shape can often be obtained for several different choices of star vectors and bond strengths. Selection of bond directions and strengths which result in a particular Wulff shape is a somewhat hit-or-miss procedure. It is known that the directions of the cusps in the γ plot are given by Eq. (9). Therefore, one can choose the bond directions to ensure that there is a cusp whose direction is normal to each facet in the desired ES. However, it is usually unavoidable that many other cusps are created as well, so one has to adjust the coefficients $g^{(\mu)}$ until these additional cusps are rendered passive. The lack of independent control over the value of $\gamma(\hat{n})$ for each icosahedral set of cusp directions greatly hinders this procedure.

(1) $N_f = 12$ (*pentagonal dodecahedron*). In Sec. III it was mentioned that when there is one set of vectors in Eq. (8), lying along the twofold axes of an icosahedron, the Wulff construction produces the 62-faceted ES shown in Fig. 4(c). Note that if the large facets normal to the fivefold axes were expanded at the expense of the other facets, the shape would become a pentagonal dodecahedron. This effect can be achieved by introducing a second set of vectors, lying along the V_6 directions. Figure 4 shows a series of ES's obtained from these two sets of bond directions as the ratio

$$\beta(V_6, E_{15}) = g(V_6)/g(E_{15}) \quad (20)$$

is varied between +1.0 [Fig. 4(a)] and -1.2 [Fig. 4(f)]. For $\beta(V_6, E_{15})$ positive, the number of facets is constant, as one would expect from theorem 2. The trivial case $\beta(V_6, E_{15}) = 0$ is illustrated in Fig. 4(c). As $\beta(V_6, E_{15})$ is made progressively more negative, the facets which do not lie normal to a fivefold axis become smaller, and for $\beta(V_6, E_{15}) \lesssim -1.2$ are completely suppressed; in this limit the ES is the dodecahedron.

Recall that each coefficient g entering Eq. (20) depends not only on the bond strength, ϵ , but also on the rail density, σ [see Eq. (19)]. To evaluate how reasonable the models are physically, it is instructive to directly compare the repulsive versus attractive bond strengths necessary to produce a dodecahedral ES. Let us assign equal energies $\epsilon(V_6) < 0$ to bonds through the faces associated with the two sets of rails which lie along directions in V_6 , $\epsilon(F_{10}) = 0$ for the F_{10} rails, and $\epsilon(E_{15}) > 0$ for the E_{15} rails. When the greater density of repulsive rails (see Table I) is taken into account, it is found that the dodecahedron is the ES for $\epsilon(V_6)/\epsilon(E_{15}) \lesssim -0.16$. This ratio

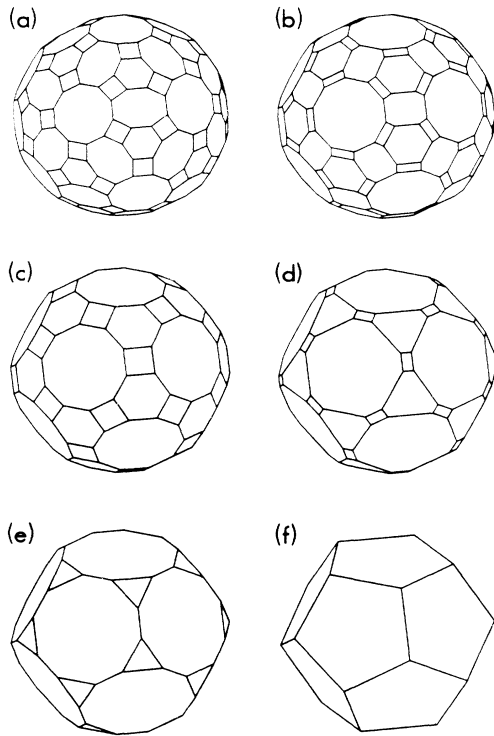


FIG. 4. Equilibrium shapes produced by two sets of vectors, E_{15} and V_6 , for various choices of lattice bond strengths. The values of $\beta(V_6, E_{15})$ [see Eq. (20) for details] are (a) 1.0, (b) 0.4, (c) 0.0, (d) -0.4 , (e) -0.8 , and (f) -1.2 .

suggests that even relatively weak repulsive interactions may be sufficient to yield a dodecahedral shape.

(2) $N_f = 20$ (*icosahedron*). Examining Fig. 4(c) once again, it can be seen that expanding the hexagonal facets while shrinking the others will eventually produce an icosahedron. However, the obvious approach of setting $A^{(1)} = E_{15}$ and $A^{(2)} = F_{10}$ does not result in this shape. The ES's produced by this choice are shown in Fig. 5, where $\beta(F_{10}, E_{15})$ ranges from $+1.0$ [Fig. 5(a)] to -0.6 [Fig. 5(d)], below which there is no further change in the shape. [The case $\beta(F_{10}, E_{15}) = 0$ is identical to Fig. 4(c).] One can deduce from Fig. 5(d) that the cusps pointing along the fivefold axes lie sufficiently close to the threefold axes that they are not moved outward to any significant degree when $\beta(F_{10}, E_{15})$ is decreased. The pentagonal facets may be suppressed by the addition of a third set of bond directions $A^{(3)} = V_6$ with a small positive coefficient $g(V_6)$. Figure 6 shows ES's for $\beta(V_6, E_{15})$ held fixed at 0.2 , while $\beta(F_{10}, E_{15})$ is decreased from -0.6 to -1.5 . The repulsive rail energies required to obtain the limiting shape, the icosahedron [Fig. 6(d)], are larger than for the case of the dodecahedron: $\epsilon(F_{10})/\epsilon(E_{15}) \lesssim -0.58$.

(3) $N_f = 30$ (*rhombic triacontahedron*). We have already seen that this shape [Fig. 7(a)] can be obtained with pure-attractive interactions from a single set of vectors $A^{(1)} = V_6$.

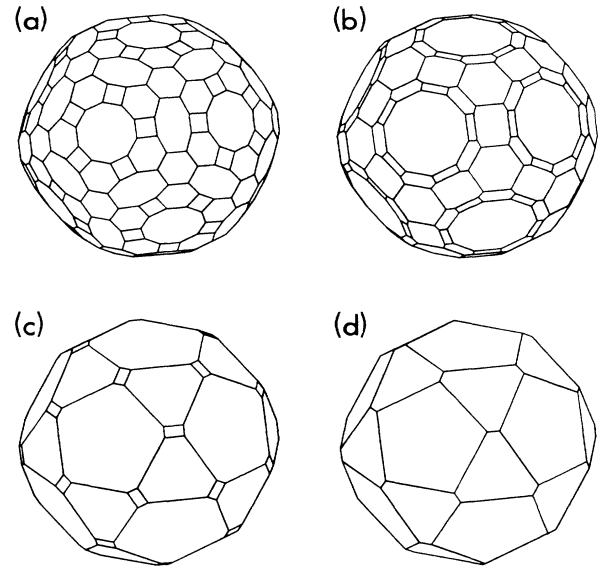


FIG. 5. Equilibrium shapes produced by two sets of vectors, E_{15} and F_{10} , for various choices of lattice bond strengths. The values of $\beta(F_{10}, E_{15})$ [see Eq. (20) for details] are (a) 1.0, (b) 0.3, (c) -0.4 , and (d) -0.6 .

(4) $N_f = 31$ (*icosidodecahedron*). Various shapes with 32 facets have already been illustrated in Figs. 4(e), 5(d), 6(b), and 6(c). The icosidodecahedron [Fig. 7(b)], like the icosahedron, may be obtained from the shape in Fig. 5(d) by the addition of bonds along the fivefold axes. In this case, however, the coefficient $g(V_6)$ is chosen to be nega-

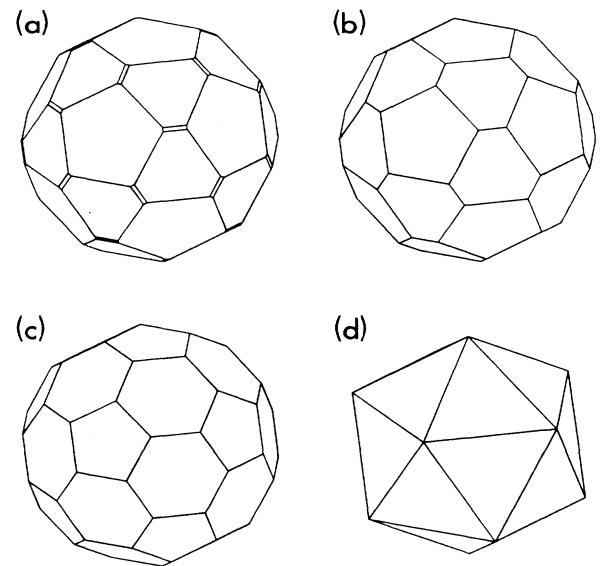


FIG. 6. Equilibrium shapes produced by three sets of vectors, E_{15} , F_{10} , and V_6 , for various choices of lattice bond strengths. The values of $\beta(F_{10}, E_{15})$ [see Eq. (20) for details] are (a) -0.6 , (b) -1.0 , (c) -1.3 , and (d) -1.5 ; in all cases, $\beta(V_6, E_{15}) = 0.2$.

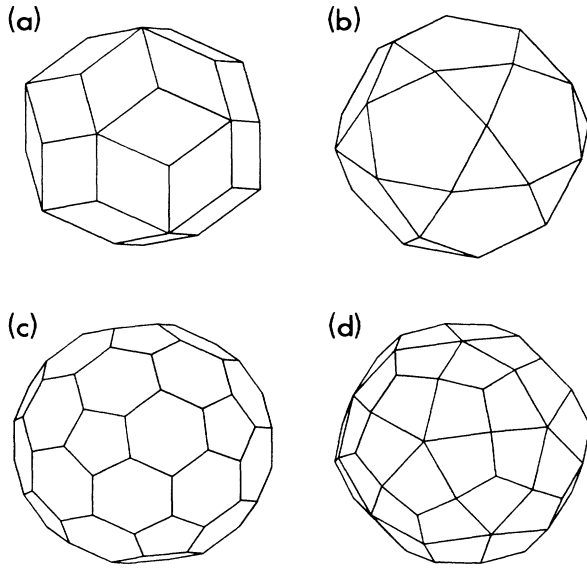


FIG. 7. Further equilibrium shapes obtained from the icosahedral quasicrystal lattice model: (a) $N_f=30$, (b) $N_f=32$, (c) $N_f=42$, and (d) $N_f=60$. We are unable to obtain $N_f=50$ for simple lattice models. Together with $n_f=12$ in Fig. 4(f), $N_f=20$ in Fig. 6(d), and $N_f=62$ in Fig. 4(c), these comprise the sequence of values of $N_f \leq 62$ consistent with icosahedral symmetry. All the shapes in this sequence, apart from those in (b) and (c), may be obtained over a finite range of parameter values.

tive. Figure 7(b) is the ES for $\beta(F_{10}, E_{15}) = -0.6$ and $\beta(V_6, E_{15}) = -0.2$.

Of all these 32-faceted shapes, only the one shown in Fig. 5(d) may be obtained over a finite range of parameter values; the remainder occur for specific choices of the interaction strengths.

(5) $N_f=42$. The 42-faceted shape shown in Fig. 7(c) can be obtained using four sets of bond directions: V_6 , F_{10} , E_{15} , and $M_{30}^{(1)}$. The equilateral shape occurs for the choice of relative bond strengths $\beta(F_{10}, V_6) \simeq 0.57$, $\beta(E_{15}, V_6) \simeq 0.17$, and $\beta(M_{30}^{(1)}, V_6) \simeq -0.40$. Since this ES requires the $M_{30}^{(1)}$ bond directions, the star which defines microscopic model must be expanded to include the F_{10} , as well as E_{15} , set of vectors.

(6) $N_f=50$. We have found no simple choice of vectors $\hat{A}_\alpha^{(\mu)}$ and coefficients $g^{(\mu)}$ which leads to a 50-faceted Wulff shape, even though such shapes are allowed by general symmetry considerations.

(7) $N_f=60$. There is no unique set of face orientations for the case $N_f=60$ because there are infinitely many distinguishable 60-member icosahedral orbits. Figure 7(d) shows the limiting Wulff shape for the F_{10} and V_6 sets of bond directions, when $\beta(V_6, F_{10}) \lesssim -0.6$. The facets are normal to the $M_{30}^{(1)}$ directions.

(8) $N_f=62$ (*great rhombicosidodecahedron*). We have already seen that this shape [Fig. 4(c)] is the ES for a single set of vectors $A^{(1)} = E_{15}$.

VI. DISCUSSION AND CONCLUSION

We have introduced a lattice model for quasicrystals which incorporates both attractive and repulsive finite-range two-body interactions. We believe that such lattice models, while not meant to be physically realistic, provide a useful theoretical approach for the study of faceting in quasicrystals. One is led to an expression for the macroscopic interfacial free-energy density at $T=0$ which is a generalization of the form derived in previous analyses of equilibrium faceting in the icosahedral phase. The ES's which may be obtained from this free energy, using the Wulff construction, include a number of simple shapes which we have proved can never arise from lattice models with pure-attractive interactions. In particular, the pentagonal dodecahedron, which is the grain shape of the thermodynamically stable icosahedral phases of Al-Cu-Fe and Ga-Mg-Zn, is a possible ES of our model.

We have shown that the addition of terms with negative coefficients to the expression for $\gamma(\hat{n})$ can result in icosahedrally symmetric ES's having fewer facets than is possible when only positive coefficients are permitted. This result is independent of the details of the microscopic model. In apparent contrast, the ES with fewest facets for a system with crystallographic symmetry is obtainable using only one set of bond directions (the smallest axis set consistent with the full point-group symmetry); the addition of terms with negative coefficients does not alter the ES.⁶

The behavior of crystalline versus quasicrystalline systems becomes consistent when one considers what is happening to the Wulff plot. Any point of the γ plot may be categorized as contributing to the ES, noncontributing, or marginal. (A marginal point is one which does not contribute a normal direction to the Wulff shape, but which would contribute if it were shifted infinitesimally towards the origin of the γ plot.) Starting with $\gamma(\hat{n})$ given by Eq. (8) with all coefficients positive, every point cusp of the γ plot contributes a facet to the polyhedral ES, and all other points are marginal. The effect of adding terms with negative coefficients is always to draw certain regions of the Wulff plot inwards towards the origin. Any change in the ES results not from an overall contraction of the γ plot by a constant scale factor, but from differences between the fractional decrease in $\gamma(\hat{n})$ along various directions \hat{n} .

In the crystallographic case, pure-attractive interactions result in the ES with the fewest possible facets. On the addition of repulsive bonds, whatever their orientation, the fractional decrease in the radius from the origin of the original cusps is as great, or greater than, that of any other point; therefore, the Wulff shape is unchanged. In the icosahedral case, pure-attractive bonds result in an ES with more than the minimal number of facets. As for the crystallographic case, repulsive interactions move certain regions of the Wulff plot inwards. However, some cusps which contributed facets to the pure-attractive ES may not move inwards sufficiently far to remain contributing points, and as a result, their facets disappear. The process can continue, as the repulsive contribution to $\gamma(\hat{n})$ is increased, until one obtains the minimal number of facets consistent with the symmetry.

At this stage, further experimental work is needed to determine whether the faceting shapes that have been observed are the same as those that would be obtained under equilibrium growth conditions. If this were the case, then the important role played by repulsive interactions in accounting for the occurrence of the pentagonal dodecahedral shape might provide some insight into the atomic structure within these materials. To date there has been little progress in the determination of the atomic structure of the icosahedral phase from diffraction data. A fundamental theoretical problem is the fact that the diffraction pattern cannot generally be separated into the lattice factor and the structure factor, which contains in-

formation about the unit-cell decoration. It may be that clues from the faceting of icosahedral phases can provide information about atomic bonds on a microscopic scale and, thereby, distinguish among atomic structural models.

ACKNOWLEDGMENTS

We wish to thank Stellan Ostlund for several helpful discussions, and Jason Ho and Dov Levine for useful suggestions. This work was supported in part by the U.S. National Science Foundation Materials Research Laboratory Program, under Grant No. DMR-85-19059.

-
- ¹B. Dubost, J. M. Lang, M. Tanaka, P. Sainfort, and M. Audier, *Nature (London)* **324**, 48 (1986).
²P. Guyot, *Nature (London)* **326**, 640 (1987).
³F. W. Gayle, *J. Mater. Res.* **2**, 1 (1987).
⁴A.-P. Tsai, A. Inoue, and T. Masumoto, *Jpn. J. Appl. Phys. Pt. 2* **26**, L1505 (1987).
⁵W. Ohashi and F. Spaepen, *Nature (London)* **330**, 555 (1987).
⁶C. Rottman and M. Wortis, *Phys. Rep.* **103**, 59 (1984).
⁷G. Wulff, *Z. Kristallogr.* **34**, 449 (1901).
⁸C. Herring, *Phys. Rev.* **82**, 87 (1951).
⁹C. Herring, in *Structure and Properties of Solid Surfaces*, edited by R. Gomer and C. S. Smith (University of Chicago Press, Chicago, 1953), pp. 5–72.
¹⁰W. K. Burton, N. Cabrera, and F. C. Frank, *Philos. Trans. R. Soc. London, Ser. A* **243**, 299 (1951).
¹¹W. W. Mullins, in *Metal Surfaces: Structure, Energetics and Kinetics* (American Society for Metals, Metals Park, OH 1963), pp. 17–66.
¹²D. Levine and P. J. Steinhardt, *Phys. Rev. B* **34**, 596 (1986).
¹³J. E. S. Socolar and P. J. Steinhardt, *Phys. Rev. B* **34**, 617 (1986).
¹⁴T. L. Ho, J. A. Jaszczak, Y. H. Li, and W. F. Saam, *Phys. Rev. Lett.* **59**, 1116 (1987).
¹⁵A. Garg and D. Levine, *Phys. Rev. Lett.* **59**, 1683 (1987).
¹⁶R. Lipowsky and C. L. Henley, *Phys. Rev. Lett.* **60**, 2394 (1988).
¹⁷J. Toner (private communication).
¹⁸D. Schechtman and I. Blech, *Metall. Trans.* **16A**, 1005 (1985).
¹⁹P. W. Stephens and A. I. Goldman, *Phys. Rev. Lett.* **56**, 1168 (1986).
²⁰K. Ingersent and P. J. Steinhardt, *Phys. Rev. Lett.* **60**, 2444 (1988).
²¹H. S. M. Coexter, *Regular Polytopes* (Pitman, New York, 1947), pp. 27 and 28.
²²J. E. S. Socolar, P. J. Steinhardt, and D. Levine, *Phys. Rev. B* **32**, 5547 (1985).
²³We adopt the nomenclature introduced in Ref. 15. The same structures are called *rows* in Ref. 16.